Check for updates

$Cu_3(PO_4)_2$: Novel Anion Convertor for Aqueous Dual-Ion Battery

Haoxiang Yu[1,2], Chenchen Deng[1], Huihui Yan[1], Maoting Xia[1], Xikun Zhang[1], Zhen-Bo Wang[2] ✉, Jie Shu[1,3] ✉

HIGHLIGHTS

- A novel anion electrode $Cu_3(PO_4)_2$ is proposed at the first time.

- The reaction mechanism of $Cu_3(PO_4)_2$ electrode is investigated.

- The dual-ion cell is constructed by using pretreated $Cu_3(PO_4)_2$ and $Na_{0.44}MnO_2$.

ABSTRACT Electrode materials which can reversibly react with anions are of interest for aqueous dual-ion batteries. Herein, we propose a novel anion electrode, $Cu_3(PO_4)_2$, for constructing an aqueous dual-ion cell. The $Cu_3(PO_4)_2$ electrode can operate in a quasi-neutral condition and deliver a reversible capacity of 115.6 mAh g^{-1} with a well-defined plateau at -0.17 V versus Ag/AgCl. Its reaction mechanism shows that $Cu_3(PO_4)_2$ decomposes into Cu_2O and subsequently is converted into Cu during the initial discharge process. In the following charge process, Cu is oxidized into Cu_2O. It suggests $Cu_3(PO_4)_2$ reacts with OH^- ions instead of PO_4^{3-} ions after the initial discharge process and its potential thereby depends upon the OH^- ions concentration in electrolyte. Additionally, an aqueous dual-ion cell is built by using pretreated $Cu_3(PO_4)_2$ and $Na_{0.44}MnO_2$ as anode and cathode, respectively. During cycling, OH^- ions and Na^+ ions in electrolyte can be stored and released. Such a cell can provide a discharge capacity of 52.6 mAh g^{-1} with plateaus at 0.70 and 0.45 V, exhibiting the potential of application. This work presents an available aqueous dual-ion cell and provides new insights into renewable energy storage and adjustment of the OH^- ions concentration in aqueous buffer solution.
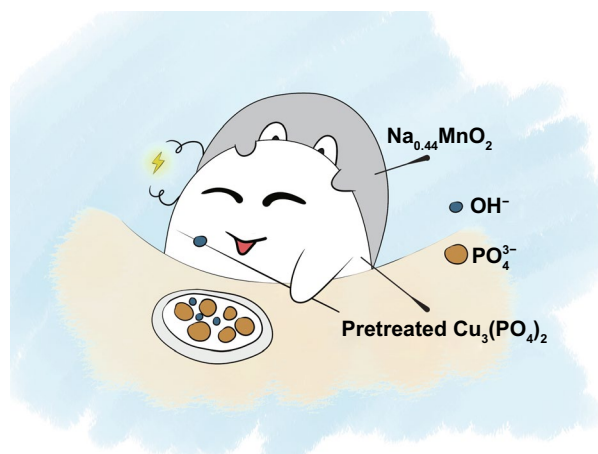
KEYWORDS Dual-ion battery; Aqueous electrolyte; $Cu_3(PO_4)_2$; Electrochemistry; Three-electrode cell

Haoxiang Yu and Chenchen Deng have contributed equally to this work.

✉ Zhen-Bo Wang, wangzhb@hit.edu.cn; Jie Shu, shujie@nbu.edu.cn

[1] School of Materials Science and Chemical Engineering, Ningbo University, Ningbo 315211, Zhejiang, People's Republic of China

[2] MIIT Key Laboratory of Critical Materials Technology for New Energy Conversion and Storage, School of Chemistry and Chemical Engineering, State Key Lab of Urban Water Resource and Environment, Harbin Institute of Technology, Harbin 150001, Heilongjiang, People's Republic of China

[3] Key Laboratory of Advanced Energy Materials Chemistry (Ministry of Education), College of Chemistry, Nankai University, Tianjin 300071, People's Republic of China

1 Introduction

For the storage of energy coming from renewables such as solar and wind, numerous efforts have been dedicated to the development of rechargeable battery over past several decades [1, 2]. Among the multitudinous explored rechargeable batteries, aqueous dual-ion battery as the novel energy storage device has attracted intensive attention recently because of its availability, low cost, high safety and eco-friendliness [3–6]. Its concept is different from that of tradition rocking-chair battery in which anions or cations migrate across electrolyte and then react with anode and cathode [7, 8]. For aqueous dual-ion battery, anions react reversibly with the electrode, whereas cations do the same way in the other electrode. It is developed from dual-carbon batteries or dual-graphite batteries as scientists find that anions can be inserted into graphite [9, 10]. The first prototype of dual-ion batteries used nonaqueous electrolytes and carbonaceous electrodes are proposed by McCullough et al. [11]. In that patent, the electrochemical behavior of this battery is described according to the "dual-intercalation" mechanism. Thereafter, continuous progress is made to the development of dual-ion batteries [12–14]. Although traditional dual-ion batteries using organic electrolytes (including ionic liquid electrolytes) exhibit high safety, high working voltages (normally > 3 V), and reasonable specific capacity (~ 80 mAh g^{-1}), the flammability and toxicity of organic electrolytes make them suffer from the safety issues [13, 15–22]. These problems hinder their wide application. To solve these problems, dual-ion batteries with nonflammable and low toxicity aqueous electrolytes have been proposed, and several configurations such as Ag/MnO$_2$ [23], NaTi$_2$(PO$_4$)$_3$/Bi [24], and NaTi$_2$(PO$_4$)$_3$/Ag [25, 26] have been demonstrated and fabricated so far. Notably, these reported systems use silver (Ag) and bismuth (Bi) as the electrodes to capture the anions. Although the performance of these materials shows decent, they possess several drawbacks which need to be conquered. Ag is a little bit expensive in price, whereas Bi can hardly react with anions in a mild solution. Thus, constructing an available aqueous dual-ion battery which can cycle in a quasi-neutral condition is of the great importance and desired.

The update of aqueous dual-ion battery depends on the selection of electrode materials which acts as its key components. Many literatures have reported the electrode materials for releasing/storing the cations [27, 28]. Yet studies for investigating the anion containers are relatively less. Hence, we herein demonstrate a novel anion container, Cu$_3$(PO$_4$)$_2$, for constructing an aqueous dual-ion cell. This material can operate in a quasi-neutral condition with well-defined plateaus and good performance, and its price is lower than that of Ag, although its reaction mechanism is far different from our original vision. We also use the pre-treated Cu$_3$(PO$_4$)$_2$ as anode to assemble the aqueous dual-ion cell coupled with Na$_{0.44}$MnO$_2$ as cathode. It presents well-defined operating plateaus and good cycling performance.

2 Results and Discussion

Cu$_3$(PO$_4$)$_2$ is an inorganic compound which is composed of copper cations and phosphate anions. Due to its insolubility in water, Cu$_3$(PO$_4$)$_2$ can be prepared by the facile precipitation method. The typical synthesis is described in supporting information. The as-obtained powder is sky blue material as shown in Fig. 1a. X-ray diffraction (XRD) pattern (Fig. 1b) suggests that two phases exist in this powder, which are Cu$_3$(PO$_4$)$_2$ and Cu$_3$(PO$_4$)$_2$·3H$_2$O, respectively, according to the two reference patterns. Besides, most of diffraction peaks are found to show the large full width at half maximum, indicative of its small crystallite size. The scanning electron microscope (SEM) images prove this result. As observed in Fig. S1a, b, the Cu$_3$(PO$_4$)$_2$ powder consists of countless nanosheets with thickness around 25 nm, providing large surface area to contact with the electrolyte. Additionally, the water content in this powder is measured by thermogravimetric (TG) analysis (Fig. S2). About 6% of mass is lost below 200 °C, corresponding to the elimination of the physically absorbed and zeolitic water [29].

Cu$_3$(PO$_4$)$_2$ selected as the electrode material in this work is based on its low thermodynamic solubility product [30]. We think when the Cu$_3$(PO$_4$)$_2$ electrode is discharged, Cu will be produced and subsequently a metal-sparingly soluble salt electrode is constructed until Cu$_3$(PO$_4$)$_2$ is vanished. The half reaction should be as follows:

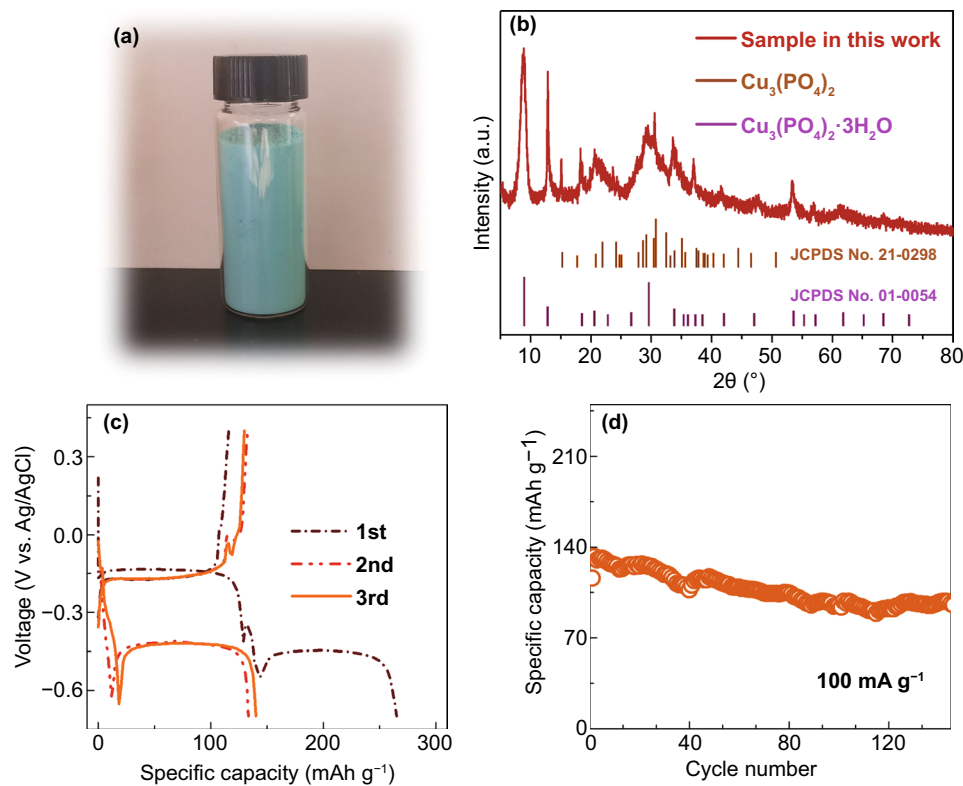$$Cu_3(PO_4)_2 + 6e^- \Leftrightarrow 3Cu + 2PO_4^{3-} \tag{1}$$

Its potential thus can be given by:

Fig. 1 **a** Digital photo and **b** XRD pattern of $Cu_3(PO_4)_2$. **c** Galvanostatic discharge/charge profiles of $Cu_3(PO_4)_2$ between -0.7 and 0.4 V versus Ag/AgCl at 100 mA g^{-1}, and **d** the corresponding cycling performance

$$E = E^\theta_{Cu^{2+}/Cu} + \frac{RT}{2F} \ln \alpha_{Cu^{2+}}$$

$$= (E^\theta_{Cu^{2+}/Cu} + \frac{RT}{6F} \ln K_{sp}) - \frac{RT}{6F} \ln \alpha^2_{PO_4^{3-}} \qquad (2)$$

$$= E^\theta_{Cu/Cu_3(PO_4)_2/PO_4^{3-}} - \frac{RT}{6F} \ln \alpha^2_{PO_4^{3-}}$$

Finally, the potential of $Cu_3(PO_4)_2$ electrode is calculated to be -0.22 V versus Ag/AgCl.

To verify the aforementioned half reaction and corresponding potential, the $Cu_3(PO_4)_2$ electrodes are fabricated and tested in three-electrode cells. Figure 1c, d exhibits the galvanostatic discharge/charge profiles of $Cu_3(PO_4)_2$ electrode and its corresponding cycling performance. Two distinct plateaus around -0.14 and -0.40 V versus Ag/AgCl is observed upon the initial discharge process, whereas only one plateau at -0.17 V versus Ag/AgCl appears in the recharge process. This case leads to that the initial discharge capacity (265.1 mAh g^{-1}) is much higher than the following recharge capacity (115.9 mAh g^{-1}). We consider that the large irreversible capacity loss during initial cycle is attributed to the formation of several intermediates as some reported metal oxides [31, 32], which can be reacted with

lithium ions in the first discharge process. Additionally, the difference between calculated potential and the experimental one is slight. In the following second and third cycles, the large irreversible capacity losses almost disappear, and the charge capacities of $Cu_3(PO_4)_2$ electrode reach to 132.6 and 129.9 mAh g^{-1}, respectively. The differential dQ/dV plots of Fig. 1c are displayed in Fig. S3. An increase in charge capacity may be owing to the fact that electrolyte does not contact well with $Cu_3(PO_4)_2$ electrode before cycling. After 45 cycles, the $Cu_3(PO_4)_2$ electrode can deliver a reversible capacity of 115.6 mAh g^{-1} with 87.2% of its second capacity. Even after 145 cycles, the reversible capacity can still be maintained at 96 mAh g^{-1}. These results suggest the good cycling performance. If any defects could be introduced into this active material, the cycling performance may be better [33, 34].

What are the intermediates during discharging and the corresponding mechanism? To answer these two questions, we have characterized the $Cu_3(PO_4)_2$ electrodes at various states of discharge by using XRD measurement. The obtained results depicted in Fig. 2 are far different
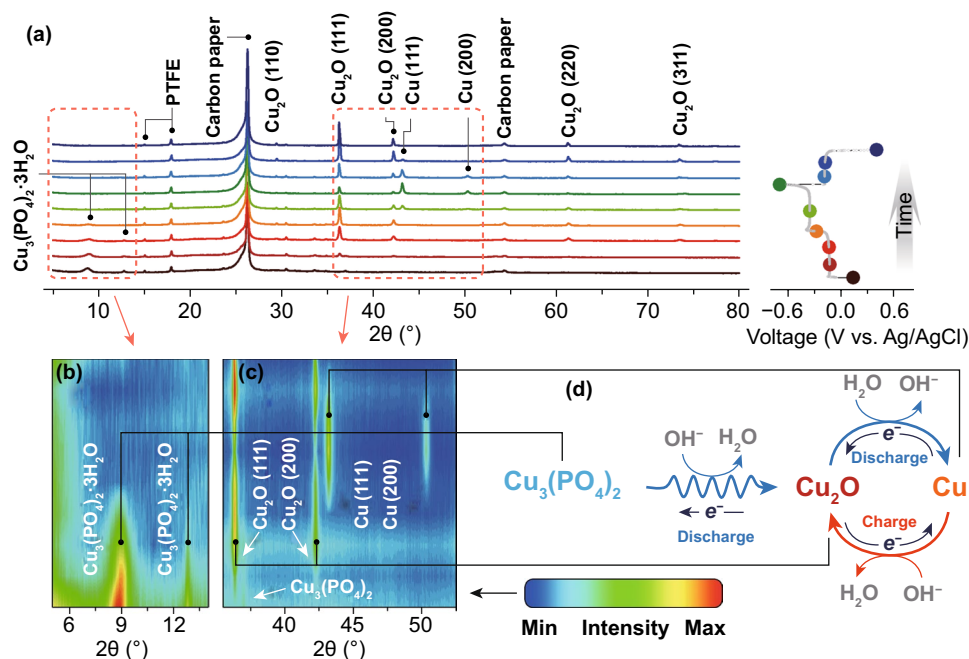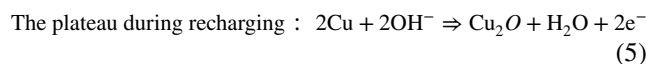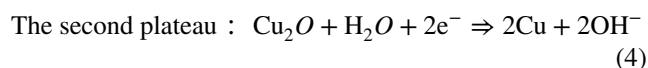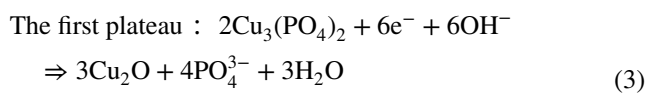
Fig. 2 **a** XRD patterns of $Cu_3(PO_4)_2$ electrode during cycling. The contour map for the corresponding XRD patterns in the 2θ range of **b** 5–14° and **c** 35.5–52.5°. **d** Reasonable mechanism for $Cu_3(PO_4)_2$ electrode during the electrochemical reaction

from our original vision. For an as-prepared $Cu_3(PO_4)_2$ electrode, diffraction peaks belonged to $Cu_{3a}(PO_4)_2$ and $Cu_3(PO_4)_2 \cdot 3H_2O$ can be defined. Since PTFE binder is electrochemically inactive, we select it as an internal standard to conduct quantitative phase analysis. With discharging to the first plateau at −0.14 V versus Ag/AgCl, the $Cu_3(PO_4)_2$ and $Cu_3(PO_4)_2 \cdot 3H_2O$ diffraction peaks in intensity slowly decrease (Fig. 2b), while two new diffraction peaks assigned to the (111) and (200) facets of Cu_2O phase appear (Fig. 2c), suggesting that the $Cu_3(PO_4)_2$ and $Cu_3(PO_4)_2 \cdot 3H_2O$ phases slowly decompose into Cu_2O. During discharging on the second plateau around −0.40 V versus Ag/AgCl, we found that the intensities of the Cu_2O diffraction peaks in electrode is still decreasing with the formation of Cu phase until the voltage is at −0.7 V versus Ag/AgCl. Thus, the intermediate upon initial discharging is Cu_2O. In the recharge process, Cu is converted into Cu_2O instead of $Cu_3(PO_4)_2$, which is the main reason for the initial irreversible capacity loss. As a result, the electrochemical reaction of the $Cu_3(PO_4)_2$ electrode during cycling can be described as:

The first plateau：$2Cu_3(PO_4)_2 + 6e^- + 6OH^-$

$$\Rightarrow 3Cu_2O + 4PO_4^{3-} + 3H_2O \tag{3}$$

The second plateau：$Cu_2O + H_2O + 2e^- \Rightarrow 2Cu + 2OH^-$

$$\tag{4}$$

The plateau during recharging：$2Cu + 2OH^- \Rightarrow Cu_2O + H_2O + 2e^-$

$$\tag{5}$$

The corresponding mechanism is schematically illustrated in Fig. 2d.

According to the electrochemical mechanism mentioned above, the $Cu_3(PO_4)_2$ electrode reacts with OH^- ions instead of PO_4^{3-} ions after initial discharge process, and its potential depends upon the concentration of OH^- ions in electrolyte. The voltage profiles of $Cu_3(PO_4)_2$ electrodes in electrolytes with different pH validate this result (Fig. S4). It should be noted that although $Cu_3(PO_4)_2$ electrode provides larger specific capacity and lower plateau in 0.75 M NaH_2PO_4 electrolyte and 0.75 M Na_3PO_4 electrolyte, respectively, their cycling performances (Fig. S5) are inferior to that of $Cu_3(PO_4)_2$ electrode in 0.75 M Na_2HPO_4 electrolyte (Fig. 1d). Nevertheless, an aqueous dual-ion cell can still be constructed and the corresponding schematic is depicted in Fig. 3a. As viewed, we select $Na_{0.44}MnO_2$ as cathode due to its low cost and eco-friendliness [35–37]. Its voltage profiles in 0.75 M NaH_2PO_4 electrolyte and 0.75 M Na_2HPO_4 electrolyte are shown in Figs. S6 and S7, respectively.
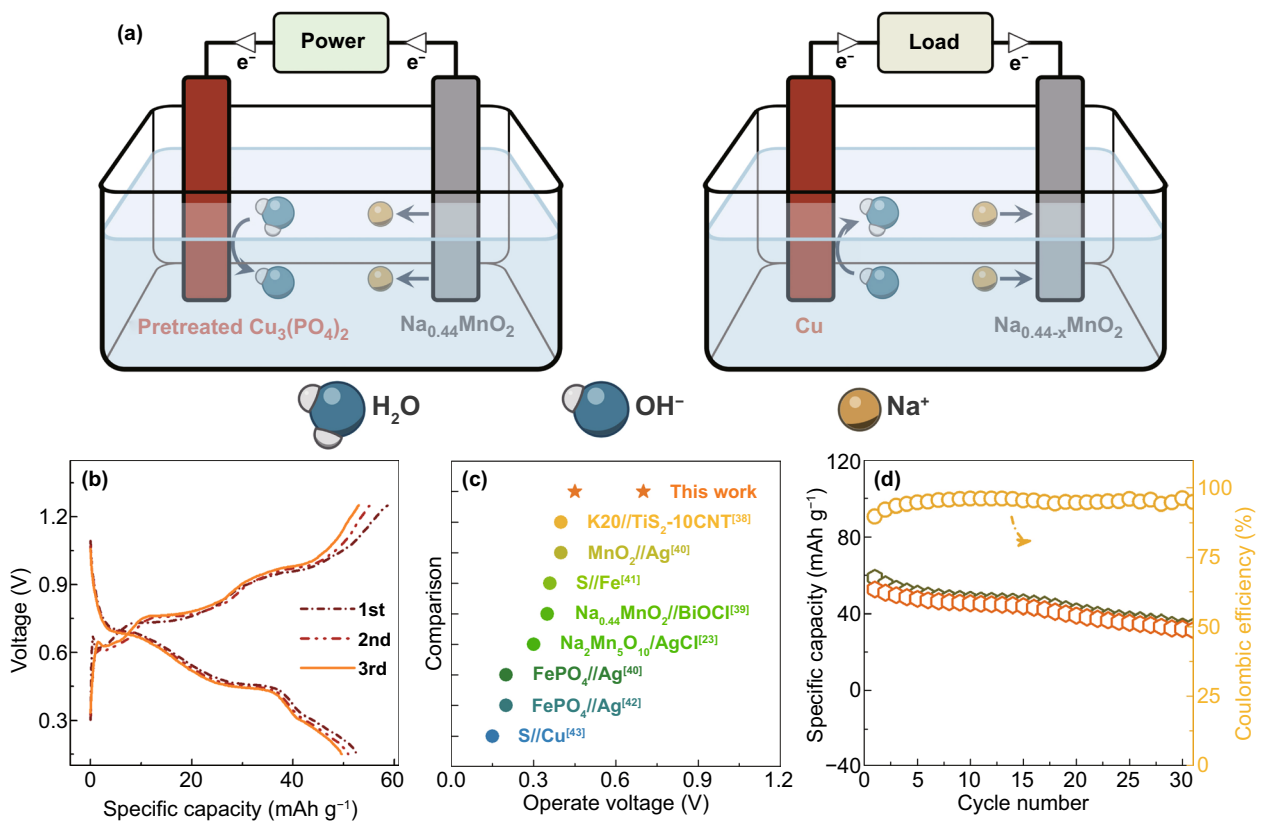
Fig. 3 **a** Schematic of pretreated $Cu_3(PO_4)_2$/$Na_{0.44}MnO_2$ dual-ion cell for charging and discharging (pretreated $Cu_3(PO_4)_2$ electrodes is that the $Cu_3(PO_4)_2$ electrodes is discharged and recharged in half cell for one cycle). **b** Galvanostatic discharge/charge profiles of pretreated $Cu_3(PO_4)_2$/$Na_{0.44}MnO_2$ dual-ion cell. **c** Operating voltage of pretreated $Cu_3(PO_4)_2$/$Na_{0.44}MnO_2$ dual-ion cell compared to the cells from previous studies. **d** Cycling performance of pretreated $Cu_3(PO_4)_2$/$Na_{0.44}MnO_2$ dual-ion cell

During charging, Na^+ ions and OH^- ions are released by the $Na_{0.44}MnO_2$ and pretreated $Cu_3(PO_4)_2$ electrodes, respectively. Meanwhile, this cell can increase the concentration of NaOH in electrolyte. Upon discharging, these two ions are captured by the cathode and anode, respectively, leading to the reduction in the concentration of NaOH. As a result, this aqueous dual-ion cell can not only modify the concentration of OH^- ions in electrolyte, but also provide electrical energy. The reaction of this cell can be written as follows:
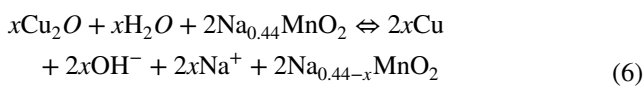
$$xCu_2O + xH_2O + 2Na_{0.44}MnO_2 \Leftrightarrow 2xCu$$
$$+ 2xOH^- + 2xNa^+ + 2Na_{0.44-x}MnO_2 \tag{6}$$

Figure 3b displays galvanostatic discharge/charge profiles of pretreated $Cu_3(PO_4)_2$/$Na_{0.44}MnO_2$ dual-ion cell. Due to the presence of irreversible capacity loss in the initial cycle, the $Cu_3(PO_4)_2$ electrode needs to be pretreated before the dual-ion cell assembly. For the pretreatment,

the $Cu_3(PO_4)_2$ electrode is discharged and subsequently recharged for 1 cycle. As observed in Fig. 3b, this as-fabricated dual-ion cell can provide a discharge capacity of 52.6 mAh g^{-1} at 0.5 C based on the mass of $Na_{0.44}MnO_2$. Thus, the x value in $Na_{0.44-x}MnO_2$ can be calculated, being 0.19. Two well-defined plateaus are observed at 0.70 and 0.45 V. By contrast, recently reported desalination batteries, such as $Na_2Mn_5O_{10}$//AgCl [23], TiS_2//K20 [38], and BiOCl//$Na_{0.44}MnO_2$ [39], displayed the operating plateaus only at ~ 0.3, ~ 0.4, and ~ 0.1 V, respectively. The detailed comparison for operating voltage of pretreated $Cu_3(PO_4)_2$/$Na_{0.44}MnO_2$ dual-ion cell in this work with other cells in the literatures [23, 38–43] is plotted in Fig. 3c and Table S1. It is worth noting that the pH value changes during cycling as shown in Fig. S8, indicating that this system can adjust the OH^- ions concentration in aqueous electrolyte. Besides, XRD patterns of $Na_{0.44}MnO_2$ in dual-ion cell during cycling are characterized as displayed in Fig. S9. The diffraction

peaks of $Na_{0.44}MnO_2$ show a quasi-regular change, suggesting that the variation of $Na_{0.44}MnO_2$ during cycling is quasi-reversible. The result is also in good agreement with previous study [44]. Figure 3d presents the cycling performance of this cell. It can retain the capacity of 43.8 mAh g^{-1} after 15 cycles. When cycled to 31 cycles, the dual-ion cell still provides 31.5 mAh g^{-1}, showing its potential of application.

3 Conclusions

In summary, we propose a novel electrode material $Cu_3(PO_4)_2$ as an anion container for aqueous dual-ion cell. The sample prepared by a simple precipitation method consists of two phases which are $Cu_3(PO_4)_2$ and $Cu_3(PO_4)_2 \cdot 3H_2O$. When tested in the three-electrode cell, it can deliver a reversible capacity of 115.6 mAh g^{-1} with a charge plateau of -0.17 V versus Ag/AgCl. Our investigation for the reaction mechanism of $Cu_3(PO_4)_2$ reveals that the initial capacity loss of this material comes from the decomposition of $Cu_3(PO_4)_2$ into Cu_2O, and such transformation is irreversible. Besides, $Cu_3(PO_4)_2$ reacts with OH^- ions instead of PO_4^{3-} ions after the initial discharge process. Eventually, an available aqueous dual-ion cell has been successfully constructed by applying pretreated $Cu_3(PO_4)_2$ and $Na_{0.44}MnO_2$ as anode and cathode. It can provide a discharge capacity of 52.6 mAh g^{-1} with plateaus at 0.70 and 0.45 V, exhibiting its potential of application. On the basis of this work, our next study shall focus on adjustment of the OH^- ions concentration in electrolyte by using this dual-ion cell.

References

1. M. Armand, J.M. Tarascon, Building better batteries. Nature **451**, 652 (2008). https://doi.org/10.1038/451652a

2. J. Meng, Z. Yang, L. Chen, H. Qin, F. Cui et al., Energy storage performance of CuO as a cathode material for aqueous zinc ion battery. Mater. Today Energy **15**, 100370 (2020). https://doi.org/10.1016/j.mtener.2019.100370

3. X. Zhou, Q. Liu, C. Jiang, B. Ji, X. Ji et al., Strategies towards low-cost dual-ion batteries with high performance. Angew. Chem. Int. Ed. **132**, 3830 (2020). https://doi.org/10.1002/ange.201814294

4. M. Wang, Y. Tang, A review on the features and progress of dual-ion batteries. Adv. Energy Mater. **8**, 1703320 (2018). https://doi.org/10.1002/aenm.201703320

5. T. Liu, X. Zhang, M. Xia, H. Yu, N. Peng et al., Functional cation defects engineering in TiS_2 for high-stability anode. Nano Energy **67**, 104295 (2020). https://doi.org/10.1016/j.nanoen.2019.104295

6. H. Yu, X. Cheng, M. Xia, T. Liu, W. Ye et al., Pretreated commercial $TiSe_2$ as an insertion-type potassium container for constructing "Rocking-Chair" type potassium ion batteries. Energy Storage Mater. **22**, 154 (2019). https://doi.org/10.1016/j.ensm.2019.01.010

7. J.M. Tarascon, M. Armand, Issues and challenges facing rechargeable lithium batteries. Nature **414**, 359 (2001). https://doi.org/10.1038/35104644

8. B. Dunn, H. Kamath, J. Tarascon, Electrical energy storage for the grid: a battery of choices. Science **334**, 928 (2011). https://doi.org/10.1126/science.1212741

9. M. Inagaki, Applications of graphite intercalation compounds. J. Mater. Res. **4**, 1560 (1989). https://doi.org/10.1557/JMR.1989.1560

10. V.W. Rüdorff, U. Hofmann, Über Graphitsalze. Z. Anorg. Allg. Chem. **238**, 1–50 (1938). https://doi.org/10.1002/zaac.19382380102

11. F.P. McCullough, C.A. Levine, R.V. Snelgrove, Secondary battery (Dow Chemical Co.), US4830938, (1989)

12. J.R. Dahn, J.A. Seel, Energy and capacity projections for practical dual-graphite cells. J. Electrochem. Soc. **147**, 899 (2000). https://doi.org/10.1149/1.1393289

13. J. Fan, Z. Zhang, Y. Liu, A. Wang, L. Li et al., An excellent rechargeable PP14TFSI ionic liquid dual-ion battery. Chem. Commun. **53**, 6891 (2017). https://doi.org/10.1039/c7cc02534c

14. G. Wang, F. Wang, P. Zhang, J. Zhang, T. Zhang et al., Polarity-switchable symmetric graphite batteries with high energy and high power densities. Adv. Mater. **30**, 1802949 (2018). https://doi.org/10.1002/adma.201802949

15. T. Placke, O. Fromm, S.F. Lux, P. Bieker, S. Rothermel et al., Reversible intercalation of bis(trifluoromethanesulfonyl)imide anions from an ionic liquid electrolyte into graphite for high performance dual-ion cells. J. Electrochem. Soc. **159**, A1755 (2012). https://doi.org/10.1149/2.011211jes

16. H. Yang, X. Shi, T. Deng, T. Qin, L. Sui et al., Carbon-based dual-ion battery with enhanced capacity and cycling stability. ChemElectroChem **5**, 3612 (2018). https://doi.org/10.1002/celc.201801108

17. Z. Li, J. Liu, J. Li, F. Kang, F. Gao, A novel graphite-based dual ion battery using PP14NTF2 ionic liquid for preparing graphene structure. Carbon **138**, 52 (2018). https://doi.org/10.1016/j.carbon.2018.06.002

18. A. Wang, W. Yuan, J. Fan, L. Li, A dual-graphite battery with pure 1-Butyl-1-methylpyrrolidinium bis(trifluoromethylsulfonyl) imide as the electrolyte. Energy Technol. **6**, 2172–2178 (2018). https://doi.org/10.1002/ente.201800269

19. Y. Huang, R. Xiao, Z. Ma, W. Zhu, Developing dual-graphite batteries with pure 1-ethyl-3-methylimidazolium trifluoromethanesulfonate ionic liquid as the electrolyte. ChemElectroChem **6**, 4681 (2019). https://doi.org/10.1002/celc.201901171

20. Y. Fang, C. Chen, J. Fan, M. Zhang, W. Yuan et al., Reversible interaction of 1-butyl-1-methylpyrrolidinium cations with 5,7,12,14-pentacenetetrone from a pure ionic liquid electrolyte for dual-ion batteries. Chem. Commun. **55**, 8333 (2019). https://doi.org/10.1039/c9cc04626g

21. Z. Lv, M. Han, J. Sun, L. Hou, H. Chen et al., A high discharge voltage dual-ion rechargeable battery using pure $(DMPI^+)$ $(AlCl_4^-)$ ionic liquid electrolyte. J. Power Sources **418**, 233 (2019). https://doi.org/10.1016/j.jpowsour.2019.02.035

22. Z. Lv, J. Sun, S. Zhou, Y. Bian, H. Chen et al., Electrochemical and physical properties of imidazolium chloride ionic liquids with pyrrolidinium or piperidinium cation addition and their application in dual-ion batteries. Energy Technol. **8**, 2000432 (2020). https://doi.org/10.1002/ente.202000432

23. M. Pasta, C.D. Wessells, Y. Cui, F.L. Mantia, A desalination battery. Nano Lett. **12**, 839 (2012). https://doi.org/10.1021/nl203889e

24. D. Nam, K. Choi, Bismuth as a new chloride-storage electrode enabling the construction of a practical high capacity desalination battery. J. Am. Chem. Soc. **139**, 11055 (2017). https://doi.org/10.1021/jacs.7b01119

25. F. Chen, Y. Huang, D. Kong, M. Ding, S. Huang et al., $NaTi_2(PO_4)_3$–Ag electrodes based desalination battery and energy recovery. FlatChem **8**, 9 (2018). https://doi.org/10.1016/j.flatc.2018.02.001

26. L. Wang, C. Mu, H. Li, F. Li, A dual-function battery for desalination and energy storage. Inorg. Chem. Front. **5**, 2522 (2018). https://doi.org/10.1039/c8qi00704g

27. Y. Yuan, Z. Chen, H. Yu, X. Zhang, T. Liu et al., Heteroatom-doped carbon-based materials for lithium and sodium ion batteries. Energy Storage Mater. **32**, 65 (2020). https://doi.org/10.1016/j.ensm.2020.07.027

28. A. Eftekhari, Z. Jian, X. Ji, Potassium secondary batteries. ACS Appl. Mater. Interfaces **9**, 4404 (2017). https://doi.org/10.1021/acsami.6b07989

29. C. Zhang, Y. Xu, M. Zhou, L. Liang, H. Dong et al., Potassium prussian blue nanoparticles: a low-cost cathode material for potassium-ion batteries. Adv. Funct. Mater. **27**, 1604307 (2017). https://doi.org/10.1002/adfm.201604307

30. J.G. Speight, *Lange's Handbook of Chemistry*, 16th edn. (The McGraw-Hill Companies Inc, United States of America, 2005).

31. D. Larcher, D. Bonnin, R. Cortes, I. Rivals, L. Personnaz et al., Combined XRD, EXAFS, and Mössbauer studies of the reduction by lithium of α–Fe_2O_3 with various particle sizes. J. Electrochem. Soc. **150**, A1643 (2003). https://doi.org/10.1149/1.1622959

32. S.H. Choi, K.Y. Jung, Y.C. Kang, Amorphous GeO_x-coated reduced graphene oxide balls with sandwich structure for long-life lithium-ion batteries. ACS Appl. Mater. Interfaces **7**, 13952 (2015). https://doi.org/10.1021/acsami.5b02846

33. Z. Su, J. Liu, M. Li, Y. Zhu, S. Qian et al., Defect engineering in titanium-based oxides for electrochemical energy storage devices. Electrochem. Energ. Rev. **3**, 286 (2020). https://doi.org/10.1007/s41918-020-00064-5

34. S. Qian, H. Chen, Z. Wu, D. Li, X. Liu et al., Designing ceramic/polymer composite as highly ionic conductive solid-state electrolytes. Batter. Supercaps **3**, 1 (2020). https://doi.org/10.1002/batt.202000149

35. T. Yuan, J. Zhang, X. Pu, Z. Chen, C. Tang et al., Novel alkaline $Zn/Na_{0.44}MnO_2$ dual-ion battery with a high capacity and long cycle lifespan. ACS Appl. Mater. Interfaces **10**, 34108 (2018)

36. Z. Li, D. Young, K. Xiang, W.C. Carter, Y. Chiang, Towards high power high energy aqueous sodium-ion batteries the $NaTi_2(PO_4)_3/Na_{0.44}MnO_2$ system. Adv. Energy Mater **3**, 290 (2013)

37. Q. Liu, Z. Hu, M. Chen, Q. Gu, Y. Dou et al., Multiangular rod-shaped Na MnO2 as cathode materials with high rate and long life for sodium-ion batteries. ACS Appl. Mater. Interfaces **9**, 3644 (2017)

38. P. Srimuk, J. Lee, A. Tolosa, C. Kim, M. Aslan et al., Titanium disulfide: a promising low-dimensional electrode material for sodium ion intercalation for seawater desalination. Chem. Mater. **29**, 9964 (2017). https://doi.org/10.1021/acs.chemmater.7b03363

39. F. Chen, Y. Huang, L. Guo, L. Sun, Y. Wang et al., Dual-ions electrochemical deionization: a desalination generator. Energy Environ. Sci. **10**, 2081 (2017). https://doi.org/10.1039/c7ee00855d

40. F.L. Mantia, M. Pasta, H.D. Deshazer, B.E. Logan, Y. Cui, Batteries for efficient energy extraction from a water salinity difference. Nano Lett. **11**, 1810 (2011). https://doi.org/10.1021/nl200500s

41. X. Wu, A. Markir, Y. Xu, E.C. Hu, K.T. Dai et al., Rechargeable iron-sulfur battery without polysulfide shuttling. Adv. Energy Mater. **9**, 1902422 (2019). https://doi.org/10.1002/aenm.201902422

42. M. Pasta, A. Battistel, F.L. Mantia, Batteries for lithium recovery from brines. Energy Environ. Sci. **5**, 9487 (2012). https://doi.org/10.1039/c2ee22977c

43. X. Wu, A. Markir, L. Ma, Y. Xu, H. Jiang et al., A four-electron sulfur electrode hosting a Cu^{2+}/Cu^{+} redox charge carrier. Angew. Chem. Int. Ed. **58**, 12640 (2019). https://doi.org/10.1002/anie.201905875

44. F. Sauvage, L. Laffont, J.M. Tarascon, E. Baudrin, Study of the insertion/deinsertion mechanism of sodium into $Na_{0.44}MnO_2$. Inorg. Chem. **46**, 3289 (2007)